

Synthesis of Gd-doped CeO₂ by ultrasonic spray pyrolysis with salt-assisted decomposition and its electrical and mechanical properties

Hee Jung Park^{a,*}, Gyung Bok Kim^b, Seng Jae Jung^b, Young-In Lee^c, Jae-Kyo Yang^d, Yun Ho Jin^d and Yong Ho Choa^{b,*}

^aDepartment of Advanced Materials Engineering, Daejeon University, 62 Daehak-ro, Dong-gu, Daejeon 300-716, Korea

^bDepartment of Fusion Chemical Engineering, Hanyang University, 55 Hanyangdaehak-ro, Sangnok-gu, Ansan 15588, Korea

^cDepartment of Materials Science and Engineering, Science & Technology, 232 Gongneung-ro, Nowon-gu, Seoul, 01811, Korea

^dAdvanced Materials & Processing Center, Institute for Advanced Engineering, 175-28, Goan-ro 51, Baejam-myeon, Yongin-si, 449-863, Korea

Much attention has been paid to acceptor doped-ceria as a promising solid electrolyte for intermediate temperature solid oxide fuel cells (IT-SOFCs) due to its high oxygen-ion conductivity. However, poor sinterability leading to high grain boundary resistance and weak mechanical properties have limited its commercialization. In this work, ceria nanoparticles were synthesized via ultrasonic spray pyrolysis using salt-assisted decomposition (SA-USP) to enhance the sinterability of the ceria. The effects of the quantity of added salt on the nanoparticle-characteristics were examined. Highly dense ceria (relative density ~97.5%) was obtained by sintering the nanoparticles at a temperature as low as 1300 °C and its mechanical and electrical properties were investigated. The hardness and the oxygen-ion conductivity of the ceria with high density were reasonably good, ~14 GPa and above 10⁻³ S/cm at the IT-SOFC operating temperatures.

Key words: USP, GDC, Density, Electrical property, Mechanical property.

Introduction

Fuel cells, which convert chemical energy into electrical energy, are expected to be next generation high-efficiency energy harvest systems and a clean energy source [1]. In particular, among various types of fuel cells, the solid oxide fuel cell (SOFC) has received much attention since it produces electricity directly, with high efficiency, by electrochemical reaction using gaseous fuel. It also uses low cost catalyst. Conventional SOFCs, however, operate at very high temperature (> 800 °C) due to the insufficient oxygen-ion conductivity of the commonly used solid electrolyte (SE) YSZ (yttria stabilized zirconia), leading to chemical/mechanical instability and high operating cost. It is generally believed that reducing the operating temperature from more than 800 °C to an intermediate temperature range of 600–700 °C is a possible solution that would allow the commercialization of SOFCs [2, 3]. The intermediate temperature (IT) would not only reduce operating costs but also effectively increase the durability of SOFCs by suppressing the interfacial reaction of cell components and the particle growths of the electrode materials. However, lower-temperature operation depends on enhanced ion conductance in the solid electrolyte, and there has been an

active search for materials with high ionic conductivity at lower temperatures [4–6].

Ceria based materials such as Gd-doped CeO₂ have recently attracted attention as potential SEs for IT-SOFC operating below 700 °C, due to their high oxygen-ionic conductivity and good compatibility with electrodes [7–11]. Its oxygen-ion conductivity is orders of higher than that of YSZ at low temperatures, so a few SOFC-companies have commercially adopted ceria for materials for their IT-SOFC [12]. However, the materials' poor sinterability has still limited their wide use as SE [13, 14].

The sinterability of SEs is one of the crucial factors affecting SOFC performance because low density SE leads to poor mechanical properties and high grain boundary (gb) resistance [13, 14]. If severely porous, the gas tight seal between electrodes could fail, resulting in the mixing of fuel and air gases together in a cell. It is known that high sintering temperatures above 1400 °C are required in order to make ceria-based materials dense [7–11]. Such high sintering temperatures result in unwanted interfacial reactions between cell components, and in the anode support-type of SOFCs, negatively affect the microstructure of the anode, which finally determines the power output of the SOFCs (note that the anode-supported type is the most popular type of SOFCs) [3, 15].

T. Suzuki et al. reported in *Science* that 1250 °C sintering of the anode-supported type leads to high open porosity (54%) of the anode and nanoparticles (< 100 nm), leading to a high performance of > 1 W/

*Corresponding author:

Tel : +82-042-280-2417

Fax: +82-042-280-2418

E-mail: hjpark@dju.kr, choa15@hanyang.ac.kr

cm² at 600 °C [3]. Therefore, other recent, significant efforts to prepare dense ceria electrolytes at reduced sintering temperature are being made. For instance, some researchers have tried to add sintering aids such as transition metal oxides (CoO, CuO, Fe₂O₃, ZnO etc.) to the ceria matrix, which reduces the sintering temperature by advancing the liquid-phase sintering of the ceria [10, 16,17]. However, the aids ultimately remain as undesired impurities within the gb and thus result in high gb resistance [10, 17]. Others have adopted the use of high activity sintering nano-sized powders synthesized by various wet chemical techniques such as sol-gel, citrate-nitrate process and co-precipitation. This approach reflects the fact that the size of the starting powders is another important factor affecting the relative density of the final ceramics (note that nano-sized or nanocrystalline powders have high surface energy, which accelerates mass diffusion transport). [18, 19]. However, finding an optimal synthetic process that can rapidly and continuously produce multi-component materials of nanometer size continues to be a challenge.

Among many methods, ultrasonic spray pyrolysis (USP) is a simple method to synthesize multi-component materials such as Gd-doped CeO₂ [20]. Synthesis of powders by USP is continuous and is expected to be applied directly to fuel cell industries since it provides low cost, chemical flexibility, and continuous production. The detailed mechanism of the USP process is explained elsewhere [21]. In general, each of the final produced particles, called secondary particles, consist of numerous nanoparticles, called primary nanoparticles. The primary particles, however, are practically inseparable due to the formation of a three-dimensional network [22]. One of the solutions proposed to separate the agglomerated primary particles from each other within the secondary particles is to add a salt into the precursor solution. This is known as a salt assisted (SA)-USP process [23]. It is known that the primary nanoparticles can be monodispersed by washing away the salt that remains in the secondary particles after synthesizing. The detailed mechanism is explained elsewhere [24]. This novel route can offer good controllability of particle size, chemical composition and material crystallinity, all of which are important for multi-component materials such as Gd-doped CeO₂.

In this work, ceria nanopowders (Ce_{0.8}Gd_{0.2}O_{2-d}, GDC) were synthesized via SA-USP. The effects of the quantity of added salt on the powders' characteristics, such as particle morphology, were examined. Additionally, the mechanical and electrical properties of the dense ceria fabricated with those nanopowders were investigated.

Experimental

To synthesize GDC nanopowders a starting precursor solution was prepared by mixing gadolinium nitrate

(gadolinium nitrate hexahydrate, metal basis, Aldrich, 99.9%), Cerium nitrate (Cerium nitrate hexahydrate, 99.0%, Aldrich), ethylene glycol (Ethylene glycol, Reagent plus, > 99.0%, Aldrich) and citric acid (Citric acid monohydrate, 99.5%, Daejung Chemical. Co.) in D.I. water. The concentration was fixed at 0.1 M. Then NaCl (Sodium chloride, 99.0%, Samchun Chemicals) as a salt was added to the solution. The weight ratios of the salt were 1, 10, and 100 of the Gd- and Ce-nitrates. Hereafter, the samples were named GDC1, GDC10 and GDC100 to reflect the relative content of the salt. During SA-USP, solution mists were generated by an ultrasonic atomizer with a frequency of 1.6 MHz and carried into the furnace which was preheated to a given temperature (800 °C). The flow rate of the carrier gas (oxygen) was 2l/min. After the synthesized powders were acquired in the outlet, they were washed with D.I. water several times to clean the salt out.

Crystal structures of the as-synthesized and washed powders were characterized by X-ray diffractometer (XRD, Rigaku,D/Max-2500). The morphology and microstructures of the nanopowders were characterized by field emission scanning electron microscopy (FE-SEM, Hitachi S-4800) and transmission electron microscope (TEM, JEOL JEM-2100F).

In order to investigate the physical properties of the GDC, pellets were prepared using conventional forming and sintering process. The green pellets were prepared by uniaxial dry pressing of the nanopowder at 200 MPa and then were sintered as a function of temperatures (from 900 °C to 1500 °C) for 5hr under air. The relative densities of the sintered samples were determined by Archimedes method. To measure the average grain size of the sintered materials, the linear-intercept method was used with SEM micrographs. The mechanical properties of the sintered pellet were measured by the Vicker's hardness method. For electrical measurements, platinum ink was painted on both sides of the pellet and heated at 800 °C for 2 h to serve not only as a current collector but also as an electrode. The electrical resistance was measured using 2-probe ac techniques as a function of temperature (250-650 °C). AC impedance spectra were obtained in the frequency range of 1 Hz to 10 MHz using an impedance analyzer (Material Mates 7260), and the measurement was swept to ensure the thermal equilibrium and stability of the sample. For the fitting of the data, the Z-view program (Scribner Associates) was used.

Results and Discussion

The solid state reaction, precipitation and Sol-gel methods are representative ceramic processing techniques used for the synthesis of SE of SOFCs [7-11]. However, it is difficult to achieve optimal powder characteristics for multi-component materials with these techniques because the materials must undergo subsequent calcination and mixing steps. Moreover, the multi-component materials

obtained by such methods may not be uniformly distributed and may be unintentionally agglomerated. These phenomena worsen as the particle size drops down to nanoscale.

SA-USP, a simple and versatile synthetic method, was implemented to obtain GDC nanopowders. As mentioned, in the SA-USP process a specific salt (NaCl) is added into a precursor solution used for ultrasonic pyrolysis. The added salt prevents the agglomeration of the primary particles (GDC nanoparticles). The final nanoparticles are obtained by washing the produced powder, which removes the salt from the secondary particles (they are composed of GDC nanoparticles and the salt). The effect of the amount of the salt on the powder characteristics was investigated and is discussed below.

Fig. 1 shows the XRD patterns of (a) as-synthesized and (b) washed powders with respect to the ratio of the added salt in the precursor (GDC1, GDC10, GDC100). As seen in Fig. 1(a) and (b), ceria with a fluorite-crystal structure and salt with a rock-salt crystal structure were well formed after synthesizing and only the ceria remained after washing (that is, the salt was completely solved out through washing). The remained ceria had a fluorite crystal structure with a lattice parameter $\sim 5.419 \text{ \AA}$, which was calculated from several peaks, indicating Gd was doped into the ceria matrix (note that the lattice parameter of pure ceria is 5.411 \AA while that of 20 mol% Gd-doped ceria is 5.420 \AA as reported) [25]. Crystallized cerias were successfully synthesized regardless of the contents of the salt as seen in Fig. 1.

On the other hand, the morphologies of GDC1, GDC10 and GDC100 were each a little different, as seen in Fig. 2. The figure exhibits SEM micrographs of the as-prepared powders as a function of the added salt. All as-prepared powders (a, b and c) had near spherical

morphologies (the spherical powders are the secondary particles). However, the average sizes of the secondary particles decreased with increasing salt content (those of GDC1, GDC10, GDC100 were $\sim 0.94 \text{ \mu m}$, $\sim 0.85 \text{ \mu m}$, $\sim 0.76 \text{ \mu m}$, respectively). This means that as more salt is added, less agglomeration of the primary particles may occur. In addition, GDC10 and GDC100 had a more spherical-like morphology than GDC1. For all samples, the primary nanoparticles were separated from the secondary particles after washing as seen in Fig. 3 (the insets show clear images of the primary nanoparticles).

In order to investigate the crystallinity and size of the nanoparticles, TEM (a,b) and SAED (c) (select-area electron diffraction) studies were conducted and are shown in Fig. 4 (GDC10 was selectively shown). Four main broad rings in the SAED-pattern correspond to (1 1 1), (2 0 0), (2 2 0) and (3 1 1) reflections of the ceria, respectively, showing that the nanoparticles had the cubic fluorite structure. Those were well consistent with the main peaks of the ceria (the XRD-pattern of Fig.1). The mean size and deviation of the crystalline material were calculated using the TEM-image, and are

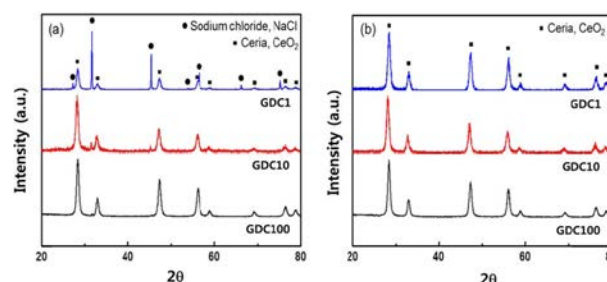


Fig. 1. X-ray diffraction patterns of GDC powders as a function of added salt in the precursor prepared by SA-USP: (a) as-prepared and (b) washed.

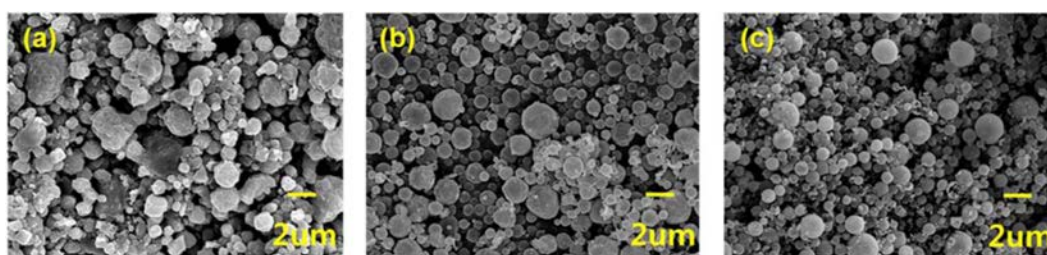


Fig. 2. FE-SEM images of as-prepared powders for a varying mixture ratio of GDC and salt in the precursor: (a) GDC1, (b) GDC10 and (c) GDC100.

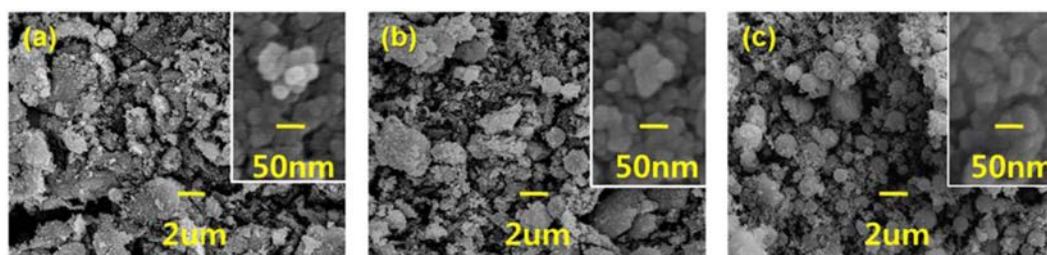


Fig. 3. FE-SEM images of washed powders for a varying mixture ratio of GDC and salt in the precursor: (a) GDC1, (b) GDC10 and (c) GDC100.

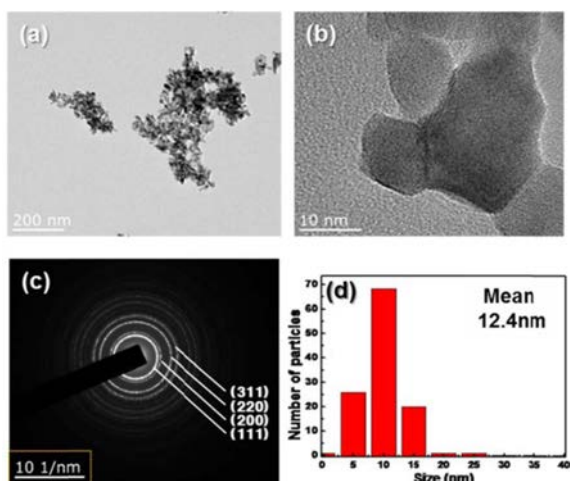


Fig. 4. (a, b) The TEM images, (c) SAED pattern and (d) size distribution of GDC10.

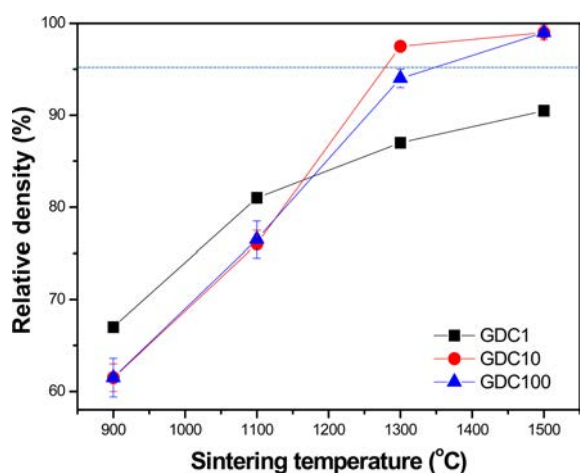


Fig. 5. Relative density of GDC1, GDC10 and GDC100 as a function of sintering temperature.

shown in Fig. 4(d). The mean computed size is ~ 12.4 nm (note that the crystalline size calculated by Scherrer's equation using XRD-peaks for GDC10 was ~ 14.5 nm after washing. Those of GDC1 and GDC100 in this study were ~ 14.9 nm and ~ 15.8 nm, respectively).

After obtaining the nanopowders of GDC through SA-USP, they were pelletized and then sintered at different temperatures (the relative densities of the green samples were in the range of 45~50%). Fig. 5 shows the relative densities of the sintered pellets as a function of sintering temperature. The relative density was measured by Archimedeian method. The dotted line corresponds to what is generally considered to be the acceptable level of sintered density (i.e, above than 95%) for use as a gas tight electrolyte membrane in SOFCs. As seen in the figure, the density increases with the increasing sintering temperature. For GDC10, it reaches up to 95% at around 1300 °C sintering temperature. In particular, the density of GDC10 sintered at 1300 °C was $\sim 97.5\%$. Nearly full densities ($\sim 99\%$) for both GDC10 and GDC100 were achieved after 1500 °C sintering. This high density of the GDC10 and GDC100 sintered materials may be attributed to good crystallinity and the nano-meter size of the starting powders. It has generally been reported that this high density is achieved above 1400 °C sintering on using the powders conventionally synthesized by solid state reaction, sol-gel process and etc [7-11].

The above relative densities were in good agreement with the microstructures taken from SEM. Fig. 6 shows images of the fractured materials of each sample sintered at 1300 and 1500 °C, respectively. It is found that GDC10 has the highest density among the samples sintered at 1300 °C and both GDC10 and GDC100 are nearly fully dense at 1500 °C sintering. The mean grain

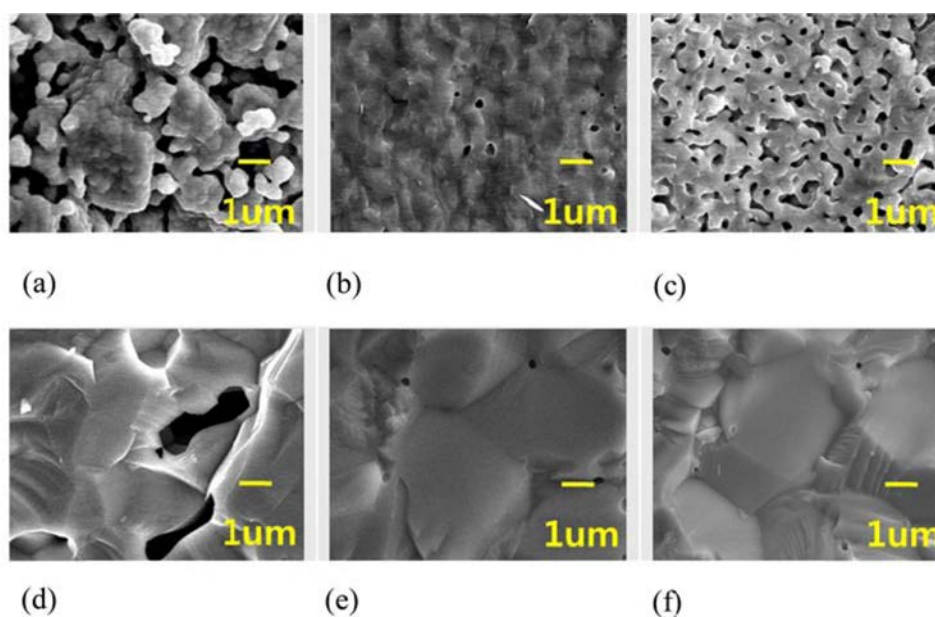


Fig. 6. Fractured SEM images of (a) GDC1, (b) GDC10 and (c) GDC100 sintered at 1300 °C, and (d) GDC1, (e) GDC10 and (f) GDC100 sintered at 1500 °C, respectively.

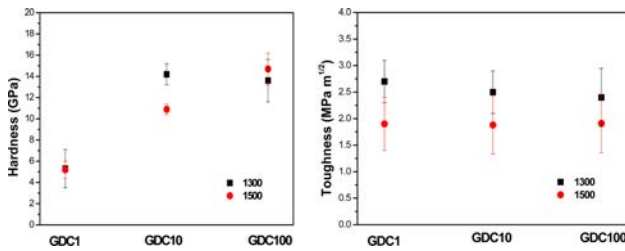


Fig. 7. (a) Vicker's hardness and (b) fracture toughness of GDC1, GDC10 and GDC100.

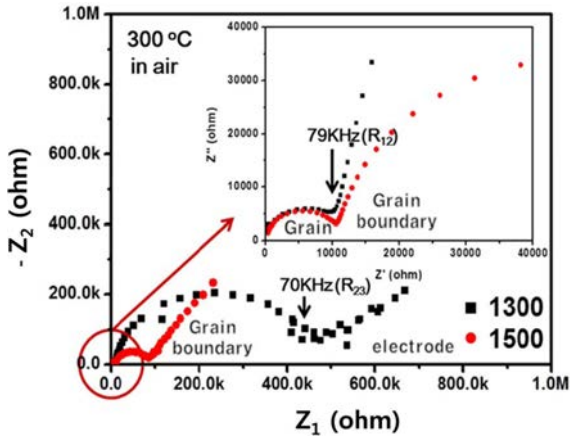


Fig. 8. The complex impedance plots of GDC10 sintered at 1300 °C and 1500 °C, respectively. Insert shows high frequency part of the impedance plot.

sizes of GDC1, GDC10 and GDC100 increased with increasing the sintering temperature. They were $\sim 0.32 \mu\text{m}$, $\sim 0.53 \mu\text{m}$ and $\sim 0.45 \mu\text{m}$ at 1300 °C sintering and $\sim 1.9 \mu\text{m}$, $\sim 2.3 \mu\text{m}$ and $\sim 2.6 \mu\text{m}$ at 1500 °C sintering in sequence of GDC1, GDC10 and GDC100, respectively.

Mechanical and electrical characteristics of some of the sintered samples were investigated as follows. Fig. 7 shows the hardness and toughness of GDC1, GDC10 and GDC100 sintered at 1300 °C and 1500 °C. The hardness increased as the density increased. This means that grain interfaces with small amounts of pores (in high density samples) became strong enough to endure the compressive stress necessary to deform the microstructure of the samples [26]. On the other hand, fracture toughness hardly depends on density (see Fig. 5). It results from differences in grain size. The fracture toughness was higher in the samples sintered at 1300 °C than at 1500 °C. The hardness and toughness measured in this study were similar or higher than the reported values. It has previously been reported that the hardness and toughness of GDC are 10 ~ 15 GPa and $1.27 \sim 1.47 \text{ MPa m}^{1/2}$ [27].

The differences in electrical properties of all samples were investigated using a 2-probe ac impedance test. Representatively, the ac results of GDC10 sintered at different temperatures (1300 °C and 1500 °C, respectively) were shown in Fig. 8 (note that GDC10 has the highest density). As seen, the typical impedance spectra of

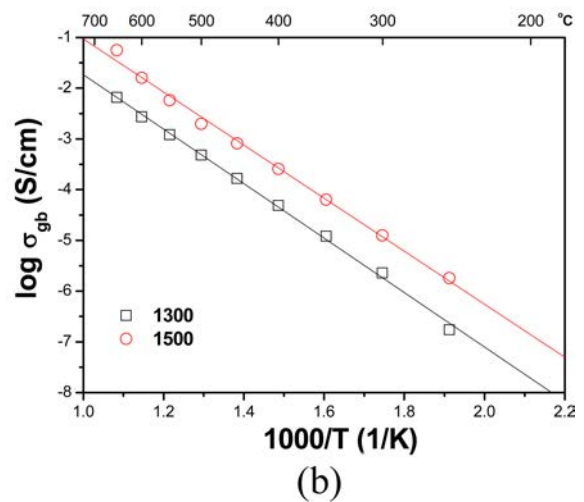
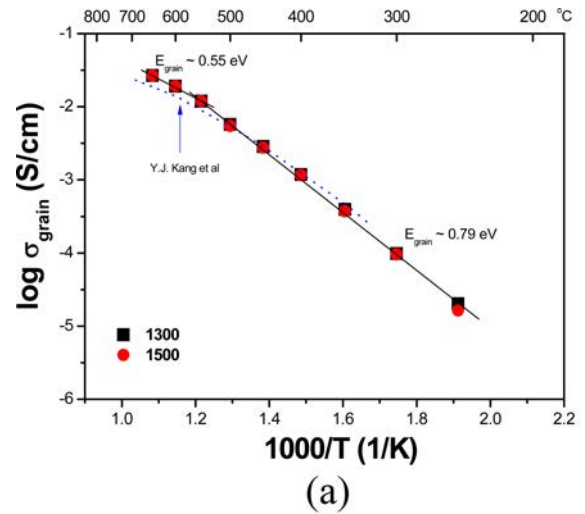


Fig. 9. (a) Grain conductivities and (b) grain boundary (gb) conductivities of GDC10 sintered at 1300 °C and 1500 °C, respectively. The dotted line in (a) is the reported grain conductivity of GDC [17].

conducting ceramics was observed. The spectrum consists of three semicircular arcs corresponding to the grain, grain boundary (gb), and electrode in that order. Those arcs are generated from the three respective resistances and capacitances (R_1C_1 - R_2C_2 - R_3C_3) of the grain, gb and electrode. The inset reveals the spectra in the higher frequency region as indicated. It was found that the sizes of the grain arcs for both samples were similar while those of the gb arcs were quite different. R_1C_1 and R_2C_2 were estimated for the grain and the gb by fitting the impedance spectrum using a corresponding equivalent circuit based on a bricklayer model. From the fits, the capacitances (C_1 and C_2) were determined to be $\sim 9 \times 10^{-12}$ and $\sim 1 \times 10^{-8-9}$ F, respectively. C_1 ensures that the semicircular arc appearing in the higher frequency region represents the grain. As seen in Fig. 8, the arc corresponding to the gb shrinks as the sintering temperature increases, indicating that the gb resistance decreases with increasing the sintering

temperature [28, 29]. This is attributed to the decrease of the gb density.

The temperature dependences of the grain conductivity (σ_{grain}) and the gb conductivity (σ_{gb}) computed from each of the resistances are exhibited in Fig. 9(a) and (b). σ_{grain} is very similar to the reported oxygen-ion conductivity of GDC, as seen [17]. Additionally, the plot of $\log \sigma_{grain}$ versus $1/T$ exhibits two linear regions with a slope change at approximately 500 °C. The change of slope is attributed to the presence of dopant ions such as Gd_{Ce}' which act not only as traps for oxygen vacancies but also as nucleating centers for the formation of ordered vacancy clusters. Accordingly, the activation energy of the grain (E_{grain}) at high temperature (> 500 °C) is the migration energy while at low temperature (< 500 °C) it is the sum of the migration energy and the association energy. Here, the migration energy is ~ 0.55 eV, which is similar to the reported value (0.6-0.7 eV), meaning that the charge carrier is surely the oxygen-ion in the grain. E_{grain} at low temperature was ~ 0.79 eV.

σ_{gb} was found to be lower than σ_{grain} , showing that the gb of GDC is resistant to the ionic transfer across them. For instance, σ_{gb} s at 600 °C was ~ 0.003 S/cm (1300 °C sintering) and ~ 0.02 S/cm (1500 °C sintering), respectively (note that σ_{grain} is ~ 0.02 S/cm at that temperature). Considering the cause, current constriction due to the pores that exist in the gb could not be a reason for the resistance, since the samples were nearly equally dense. The space charge effect may be another possible blocking source for the gb conduction [30]. In this model, charged carriers deplete or accumulate in the vicinity of the distorted grain boundary due to the space charge potential; as a result, the gb conductivities are modified. However, it is not likely that the space charge effect is responsible for the blocking since high doping makes the space charge region (depletion or accumulation region of charge carriers) small by reducing the Debye length in the gb [31]. The structural distortion of the gb is a possible explanation for the resistance. Generally, a structural effect leads to a decrease in oxygen-ion mobility and a depletion of mobile oxygen-ions. The higher activation energy of the gb (E_{gb}) than that of the grain provides further evidence. E_{gb} was ~ 1.06 eV and was ~ 1.03 eV in 1300 °C and 1500 °C sintered samples, respectively.

Total conductivities ($\sigma_{total} = \sigma_{grain} \cdot \sigma_{gb} / (\sigma_{grain} + \sigma_{gb})$) of the sintered materials at various temperatures are shown in Fig. 10. The σ_{total} of GDC10 sintered at 1300 °C is lower than that done at 1500 °C due to the higher gb resistance (see Fig. 9b). Nevertheless, the σ_{total} of GDC10 sintered at 1300 °C is not much lower than other reported values of GDCs, which were sintered above 1400 °C [7, 9, 11]. For example, H. Kim et al prepared ceria powders by using a ball-milling process and then sintered the ceria pellet at 1550 °C for 5 h (their data is inserted in Fig.10). The σ_{total} of GDC10 sintered at 1300 °C was ~ 0.003 S/cm and the value reported by Kim

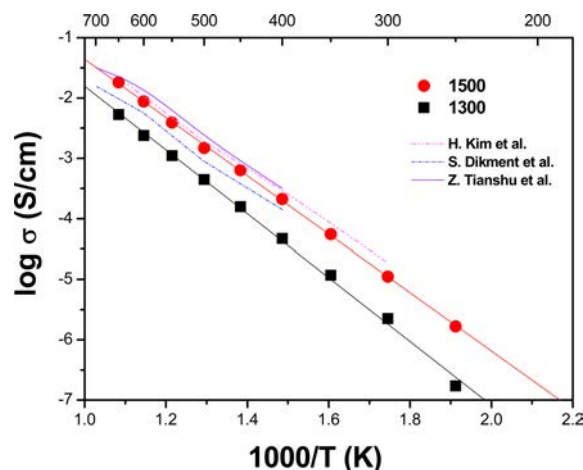


Fig. 10. Total conductivities of GDC10 sintered at 1300 °C and 1500 °C, respectively. For comparison, other reported data are inserted together.

was ~ 0.005 S/cm at 600 °C, respectively.

It was conclusively revealed that nanoparticles with multi-components can be successfully synthesized using SA-USP, enhancing the sinterability of GDC. The mechanical and electrical properties of GDC fabricated with the nanoparticles synthesized by SA-USP were quite comparable to those of samples produced by other synthesis techniques. In addition, as mentioned before, spray pyrolysis has many competitive advantages in view of processing time and cost since the powders are directly synthesized with a single continuous process, including evaporation, precipitation, decomposition and sintering stages. Therefore, synthesis by SA-USP can be a promising way to prepare ceria nanoparticles for the SE of SOFCs.

Conclusions

GDC nanoparticles were successfully synthesized via ultrasonic spray pyrolysis using salt-assisted decomposition (SA-USP). The nanoparticles enhanced the sinterability of the ceria. Nearly full density (> 97.5%) was obtained at a sintering temperature as low as 1300 °C. The mechanical and electrical properties of the GDC with high density were investigated. Those properties were reasonably good, with hardness > 10 GPa, toughness > 1.5 MPam^{1/2} and oxygen-ion conductivity > 10⁻³ S/cm at 600 °C.

Acknowledgments

This work was supported by the Korea Institute of Energy Technology Evaluation and Planning (KETEP) and the Ministry of Trade, Industry & Energy (MOTIE) of the Republic of Korea (No. 20152020105950). And we thank Jae Soo Shin and Sang Woo Kang for valuable discussion.

References

1. B.C.H. Steele and A. Heinzl, *Nature* 414 (2001) 345-352.
2. N.Q. Minh, *J. Am. Ceram. Soc.* 76 (1993) 563-588.
3. T. Suzuki, Z. Hasan, Y. Funahashi, T. Yamaguchi, Y. Fujishiro and M. Awano, *Science* 325 (2009) 852-855.
4. Z. Shao and S. Haile, *Nature* 431 (2004) 170-173.
5. W. Zhou, R. Ran and Z. Shao, *J. Power Sources* 192 (2009) 231-246.
6. H.J. Park, T.G. Kim, C. Kwak, D.W. Jung, S.M. Lee and K.H. Lee, *J. Power Sources* 275 (2015) 884-887.
7. Z. Tianshu, P. Hing, H. Huang and J. Kilner, *Solid State Ionics* 148 (2002) 567-573.
8. J.G. Cheng, S.W. Zha, J. Huang, X.Q. Liu and G.Y. Meng, *Mater. Chem. and Phys.* 78 (2003) 791-795.
9. H.N. Kim, H.J. Park and G.M. Choi, *J. Electroceram.* 17 (2006) 793-795.
10. L. Ge, R. Li, S. He, H. Chen and L. Guo, *J. Power Sources* 230 (2013) 161-168.
11. S. Dikmen, P. Shuk, M. Greenblatt and H. Gocmez, *Solid State Sciences* 4 (2002) 585-590.
12. R.T. Leah, N.P. Brandon and P. Aguiar, *J. Power Sources* 145 (2005) 336-352.
13. Y. Dong, S. Hampshire, J. Zhou and G. Meng, *Int. J. Hydrogen Energy* 36 (2011) 5054-5066.
14. Q. Lu, X. Dong, Z. Zhu and Y. Dong, *Ceramics International* 40 (2014) 15545-15550.
15. G. Constantin, C. Rossignol, J. Barnes and E. Djurando, *Solid State Ionics* 235 (2013) 36-41.
16. J.D. Nicholas and L. De Jonghe, *Solid State Ionics* 178 (2007) 1187-1194.
17. Y.J. Kang and G.M. Choi, *Solid State Ionics* 180 (2009) 886-890.
18. J. Varele, T. Horita, T. Kawada, N. Sakai, H. Yokokawa and M. Dokiya, *J. Eur. Ceram. Soc.* 16 (1996) 961-973.
19. K. Higashi, K. Sonada, H. Ono and S. Sameshima, *J. Mater. Res.* 14 (1999) 957-967.
20. V. Briois, C.E. Williams, H. Dexpert, F. Villain, B. Cabane, F. Deneuve and C. Magnier, *J. Mater. Sci.* 28 (1993) 5019-5031.
21. X. Chu, W. Chung and L.D. Schmidt, *J. Am. Ceram. Soc.* 76 (1993) 2115-2118.
22. P.L. Chen and I.W. Chen, *J. Am. Ceram. Soc.* 76 (1993) 1577-1583.
23. G.L. Messing, S.C. Zhang and G.V. Jayanthi, *J. Am. Ceram. Soc.* 76 (1993) 2707-2726.
24. G.H. An, H.J. Wang, B.H. Kim, Y.G. Jeong and Y.H. Choa, *Mat. Sci. Eng. A* 449 (2007) 821-824.
25. S. Zha, C. Xia and G. Meng, *J. Power Sources* 115 (2003) 44-48.
26. B. Huang, L.D. Chen and S.Q. Bai, *Scripta Materialia* 54 (2006) 441-445.
27. M. Morales, J.J. Roa, X.G. Gpadevila, M. Segarra and S. Pinol, *Acta Materialia* 58 (2010) 2504-2509.
28. R. Gerhardt, A.S. Nowick, M.E. Mochel and I. Dumler, *J. Am. Ceram. Soc.* 69 (1986) 641-646.
29. C. Tian and S.W. Chan, *Mater. Res. Soc. Symp. Proc.* 548 (1999) 623-640.
30. H.J. Park and S. Kim, *J. Phy. Chem. C* 111 (2007) 14903-14910.
31. X. Guo and R. Waser, *Progress in Mat. Sci.* 51 (2006) 151-210.